Received 7 October 2025, accepted 7 November 2025, date of publication 11 November 2025,
date of current version 18 November 2025.

Digital Object Identifier 10.1109/ACCESS.2025.3631517

RESEARCH ARTICLE

Knowledge Domain Control of AC/DC Hybrid Microgrid for EV Charging Application

BABITA FAUJDAR, (Graduate Student Member, IEEE),
AND RAJENDRA KUMAR PANDEY, (Senior Member, IEEE)
Electrical Engineering Department, Indian Institute of Technology (BHU), Varanasi 221005, India
Corresponding author: Babita Faujdar (babitafaujdar.rs.eee21@itbhu.ac.in)

ABSTRACT This paper presents a Knowledge Domain (KD)-based control framework for a DSTATCOM- integrated ac/dc hybrid microgrid designed for electric vehicle (EV) charging applications. The DSTATCOM, connected to the ac bus, regulates ac voltage and indirectly supports the dc bus via coordinated converter control. A small-signal model of the hybrid microgrid, including DSTATCOM dynamics, is developed to accurately capture system behavior and interactions among PV arrays, energy storage systems (ESS), EV loads, and grid-connected converters. The proposed KD control integrates offline optimization with near real-time adaptability to maintain stable EV charging under dynamically changing conditions. The controller parameters of the state feedback matrix (k) are optimized using Particle Swarm Optimization (PSO) by minimizing state deviations under perturbations via the Integral of Time-weighted Absolute Error (ITAE) criterion. The optimized parameters are stored in a KD database and mapped to operating conditions. During operation, the KD control framework rapidly retrieves appropriate parameters to update controller gains, ensuring fast damping and rapid stabilization under dynamical variations. System stability is evaluated through state perturbation analysis, where individual system states are perturbed to observe the impact on other states and verify proper settling with minimal undershoot/overshoot. A 10% dc bus voltage perturbation demonstrates that the system remains stable, with the DSTATCOM significantly reducing oscillations and settling time, which is further enhanced with PSO-tuned parameters. Experimental validation on the OPAL-RT OP4512 real-time simulator confirms the superiority of KD control over conventional PSO-tuned control, achieving faster damping, reduced settling time, and simultaneous regulation of ac and dc bus voltages. The proposed approach ensures robust microgrid operation, uninterrupted EV charging, and safe performance of interfaced converters under dynamic source and load variations.

INDEX TERMS EV charging, ac/dc hybrid microgrid, integral of time-weighted absolute error (ITAE), particle swarm optimization (PSO), DSTATCOM, knowledge domain (KD) control.

I. INTRODUCTION

The rapid rise of electric vehicles (EVs) is transforming transportation, demanding a sustainable, fast, and stable charging infrastructure. The DC microgrids, integrating solar power and energy storage systems (ESS), have emerged as a promising solution, offering reduced conversion losses and enhanced energy efficiency compared to traditional AC grids [1], [2], [3], [4], [5], [6]. However, maintaining DC grid stability remains a critical challenge, especially under dynamic load changes and intermittent renewable generation, so connecting with the edge of the AC grid is the best solution. The AC grid interface plays a vital role in balancing power, supplying the DC grid during renewable energy intermittency, and absorbing surplus power during peak generation [2], [3], and [6]. However, sudden AC load increases or DC power deficits can push the DC bus voltage beyond safe limits, destabilizing converters, stressing the AC grid, and risking the entire system, leading to collapse if advanced control concepts are not employed.

To mitigate these problems, flexible AC transmission system (FACTS) devices such as Distribution Static

The associate editor coordinating the review of this manuscript and approving it for publication was Maria Carmen Falvo.

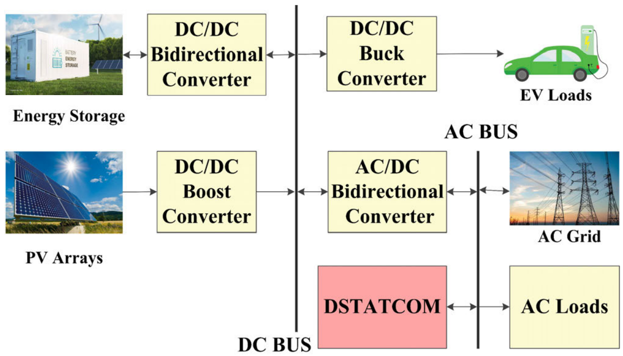

FIGURE 1. **The block diagram of the proposed DSTATCOM integrated AC/DC hybrid microgrid for EV charging application.**

Synchronous Compensators (DSTATCOM) have been widely used for dynamic voltage regulation of microgrid, and to mitigate oscillation introduced by the interaction between inverter-based resources and AC grids [7], [8], [9], [10], [11]. In [8], the DSTATCOM is used to regulate the voltage through reactive power compensation and to improve the stability of PV-wind hybrid micro-grid systems under renewable source variation. In [9], STATCOM is used to support the reactive power for frequency regulation of a wind farm-based microgrid. In [10], a PV-DSTATCOM (a D-STATCOM feeding active power through the DC link from a PV array) is used to charge the EVs and support reactive power to the AC grid to regulate the AC bus voltage. However, the literature offers a limited focus on DSTATCOM applications for EV charging. Some studies explore optimal DSTATCOM placement, while others rely on PV as the DC input of DSTATCOM, an unreliable source due to solar variability. This paper proposes a dedicated DSTATCOM control unit that ensures AC voltage regulation and indirectly stabilizes the DC bus voltage, enabling uninterrupted and high-quality EV charging.

The traditional control strategies, like PI control or PID control, often rely on fixed parameters, which may fail to adapt to changing system operating conditions, leading to oscillations and instability. The PID control provides the tuning of the controller for a particular range whenever there is a change in operating conditions or perturbations in the entire system; the tuning of PID control is a big challenge. Moreover, this tuning may not be able to reject the system disturbance or perturbation, whereas a heuristic algorithm like PSO can be used to precisely retune the controller for the best performance. The main aim of this work is to provide the best controller performance, and it can be achieved with the precise tuning of the controller over the operating range.

Heuristic algorithms have been proven to provide the best parametric tuning of controllers reported in the literature. In [12], Fire Hawk Optimization (FHO) and Hybridized Whale PSO techniques are used to optimally place the DSTATCOM and PV array for the reduction of dependency on the grid for EV charging, aiming to improve grid stability. In [13], the PSO algorithm is used to tune the control parameters of the interlinking inverter to minimize the voltage and frequency error signal, aiming to provide intelligent and optimal energy management for a microgrid under load and source generation variation. In [14], the hybrid genetic algorithm (GA) and PSO techniques are applied to optimize the controller parameter of the wind-PV- thermal-bundled power system for regulating voltage and reducing low-frequency power oscillation with STATCOM and power system stabilizers (PSS). In [15] a robust adaptive control method is applied to STATCOM to improve the small signal stability of multi-inverter-based resources (IBR) under varying operating conditions. In this paper, firstly, a set of controllers $\{K_1, K_2 \ldots, K_m\}$ have been prepared offline by solving the m optimization problem, and then, accordingly, for respective operating conditions, the proper controller K_i is chosen online to mitigate the oscillation based on real-time STATCOM output reactive current/power. In [16], a TS fuzzy approach is adopted to tune PI controllers for improved battery dynamics, while proportional gain control enhances inverter voltage stability, and a voltage-SoC-based load-shedding algorithm ensures reliable operation under contingencies, collectively providing an effective power management strategy for renewable-energy-based DC microgrids. In [17], a hybrid Firefly Algorithm (FA) and PSO method was proposed for power management within a DC microgrid, aimed at achieving faster convergence along with enhanced system stability and accuracy. The hybrid optimization technique is employed to effectively tune Takagi Sugano Fuzzy Inference Systems (TSFIS), Adaptive Neuro-Fuzzy Inference Systems (ANFIS), and Fractional Order Proportional-Integral- Derivative (FO-PID) controllers.

Across the literature, PSO has emerged as one of the leading optimization techniques for tuning control parameters in DC microgrids [10], [13], [14], and [17], owing to its balanced exploration/exploitation capability and faster convergence rate. Its application has proven effective in reducing oscillations caused by dynamic load variations and renewable generation intermittency, thereby enhancing overall system stability.

However, existing research predominantly focuses on the use of heuristic algorithms for offline or semi-static optimization of controller parameters to mitigate oscillations and improve stability [9], [10], [12], [13], [14], [16], and [17]. A critical research gap remains; limited attention has been given to maintaining stability under real-time dynamical operating conditions. Moreover, there is a lack of comprehensive analysis of the complex interactions among system components, such as PV arrays, EV charging units, energy storage systems (ESS), and the AC grid, along with their associated converters (DC/DC and DC/AC), particularly under varying and uncertain operating conditions.

To address these limitations, this paper proposes an intelligent KD-based control strategy for a DSTATCOM- integrated AC/DC hybrid microgrid supporting EV charging. The approach ensures simultaneous regulation of AC and DC

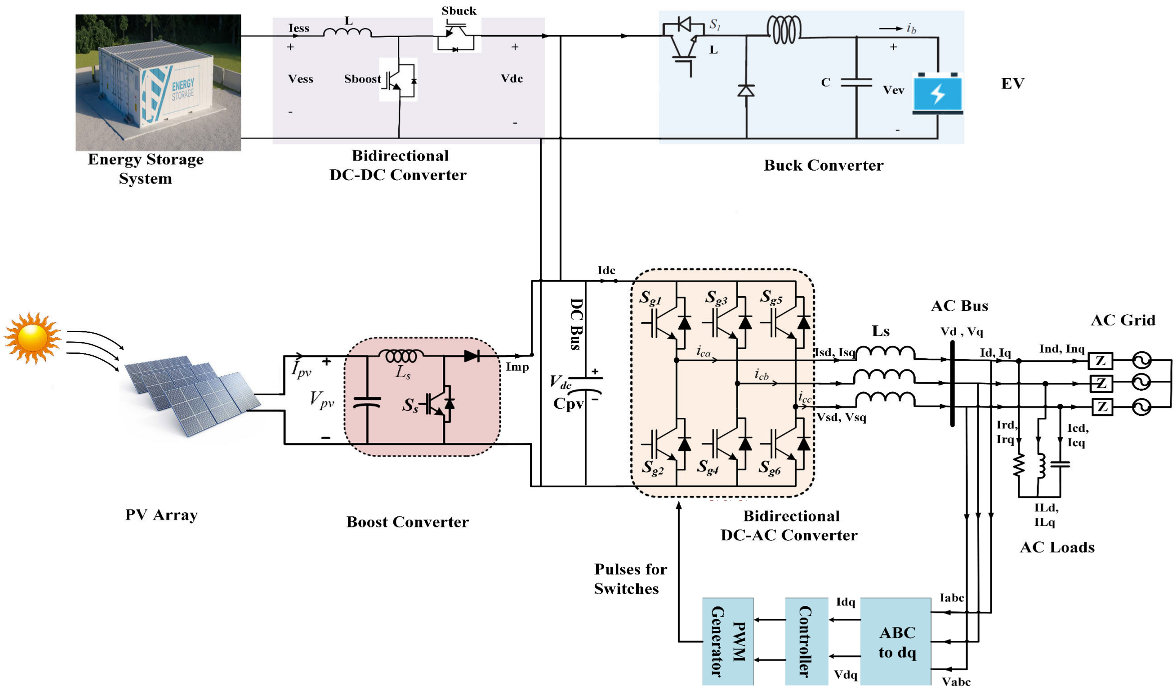

FIGURE 2. The Schematic diagram of the AC/DC hybrid microgrid for EV charging.

bus voltages and quality EV charging under varying conditions. The KD framework designs controllers for different operating conditions and stores their optimized parameters in a structured database termed as the KD database. When system dynamics change, due to PV fluctuations, load variations, or grid disturbances, the KD control framework instantaneously retrieves controller parameters and updates the state feedback control matrix gains (k), enabling smooth transitions and fast responses. This process, referred to as controller parametric updation, significantly improves the system's dynamic performance and stability.

To accurately capture system dynamics, a state-space model of DSTATCOM integrated AC/DC hybrid microgrid for EV charging has been developed. In this paper, an intelligent control strategy utilising a KD control framework has been proposed, which incorporates a combination of offline optimized control parameters using PSO with nearly real-time transition of controller realization. The PSO algorithm minimizes the state deviation using the ITAE criterion as an objective function to optimize the state feedback control matrix (k), and the results are stored in the KD database. As the operating conditions change, the KD control guided to quickly retrieve the best-fit controller parameters, thus reducing oscillations and improving overall system performance, hence ensuring resilient and stable EV charging. The key contributions of this paper are as follows:

1. Developed a small-signal model for a DSTATCOM-integrated AC/DC hybrid microgrid for EV charging, enabling accurate system dynamics analysis.
2. Analyzed dynamic interactions among PV, ESS, EV loads, and grid-connected converters, demonstrating the effectiveness of DSTATCOM and PSO-tuned control parameters in mitigating oscillations and enhancing system stability
3. Created a KD database containing PSO-optimized controller parameters for various operating conditions.
4. Implemented KD control for instantaneous parametric updates of controller gains based on system operating conditions, improving stability under dynamical variations.
5. System stability is evaluated through state perturbation analysis, where individual system states are perturbed to observe the impact on other states and verify proper settling with minimal undershoot/overshoot.
6. Experimentally validated KD control on OPAL-RT, achieving faster oscillation damping, reduced settling time, and simultaneous AC/DC bus voltage regulation compared to PSO control.

The paper is structured as follows: Section II describes the system state space model and DSTATCOM integration, Section III explains the overview of PSO-based optimization process, Section IV outlines the development of the KD control framework, Section V discusses controller tuning strategies in dynamic operating conditions, Section VI presents case studies and simulation results, and Section VII concludes with key findings and future research directions.

II. STATE SPACE MODELLING OF THE SYSTEM

A. EV CHARGING INFRASTRUCTURE MODEL

The EV charging infrastructure is powered by a photovoltaic (PV) array, ESS, and the AC grid, as shown in Fig. 2. The PV array is connected to a boost converter employing the Perturb and Observe (P&O) method for Maximum Power Point Tracking (MPPT) due to its simplicity and ease of implementation in small-signal modelling. While P&O provides a straightforward approach for representing PV dynamics, recent advanced MPPT algorithms such as Modified Adaptive Jaya Optimization (MAJO) [18] and other techniques [14], offer faster tracking and improved efficiency under varying irradiance conditions. The PV system, the ESS (connected via a bidirectional buckboost converter), and the AC grid (connected via an AC-DC bidirectional converter) are all interfaced with a common DC bus. The EV charging loads are connected directly to the DC bus through a buck converter, while AC loads are connected to the AC bus.

A small-signal model has been developed to analyse the dynamic behaviour of the system. This model is formulated by linearizing the system equations around a nominal operating point and deriving interface equations, resulting in a perturbation model with 24 states and 7 control inputs. The system dynamics are described by the state-space equation [3]:

$$\Delta\dot{x} = A\Delta x + B\Delta u \tag{1}$$

where Δx and Δu are states variable vector and control input vector respectively. The size of A matrix is 24×24, while the B matrix has 7×24. To improve the system's stability and reactive power support, DSTATCOM is connected to the AC bus.

B. D-STATCOM MODEL

The D-STATCOM is integrated into the proposed system to reduce system oscillation and improve stability by providing reactive power support for quick voltage regulation of the AC bus voltage [9], [10], [11], and [14]. During periods of high load demand, it supplies reactive power to the AC bus, while it absorbs excess reactive power during light load conditions, thereby enhancing the AC bus voltage profile. This voltage regulation indirectly stabilizes the DC bus voltage, ensuring it remains constant. Given that fluctuations in AC bus voltage can disturb the operation of the bidirectional DC-AC converter, maintaining a stable AC grid voltage is crucial to avoid possible converter control failures. The D-STATCOM is an ideal solution due to its easy installation and rapid voltage regulation capabilities.

The mathematical model of the D-STATCOM [20], [21] is developed to simulate its behaviour within the system accurately. The D-STATCOM (Fig. 3) operates as a voltage source converter (VSC), dynamically adjusting the phase angle of its injected voltage to regulate the AC bus voltage and enhance overall system stability [21]. Assuming the converter is ideal and does not have losses and harmonics, the AC grid voltage (V), expressed as the combination of d and q-axis components (V_{d} and V_{q}), is related to the DC link voltage (V_{dc_s}) of the VSC through the modulation index (m) and phase angle (δ), as shown in the equation:

$$V = Vd + jV_{\mathrm{q}} = amV_{\mathrm{dc}\_s}e^{j\delta} \tag{2}$$

The $\propto$ is the ratio between AC and DC voltage, depending on the converter structure. For a lossless converter, the instantaneous power at the AC side terminal and DC side terminal is equal, so

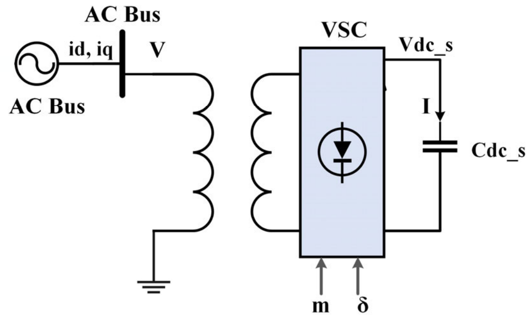

FIGURE 3. The schematic diagram of DSTATCOM.

$$V_{dc\_S}I = V_d i_d + V_q i_q \tag{3}$$

The current flow in the capacitor can be written as

$$C_{dc\_s}\frac{dV_{dc\_S}}{dt} = I \tag{4}$$

From equations (2), (3), and (4), we can write the DC link voltage of VSC as

$$\frac{dV_{dc\_S}}{dt} = \frac{km}{C_{dc\_S}}\begin{bmatrix}\cos\delta & \sin\delta\end{bmatrix}\begin{bmatrix}i_d \\ i_q\end{bmatrix} \tag{5}$$

After linearising and perturbating the equation around the nominal operating point, equation (5) becomes

$$\frac{d\Delta V_{dc\_S}}{dt} = a_{181}\Delta i_d + a_{182}\Delta i_q + b_{181}\Delta\delta + b_{182}\Delta m \tag{6}$$

Equation (6) shows that V_{dc_S} is the new state vector, which is influenced by the current injected into the AC grid, along with the control inputs δ (phase angle) and m (modulation index). Consequently, the state equation consists of 25 state variables and 9 control inputs, representing the system's dynamics and allowing for effective regulation of the AC grid voltage and DC bus voltage stability.

$$\Delta\dot{x}_{new} = A_{new}\Delta x_{new} + B_{new}\Delta u_{new} \tag{7}$$

where $\Delta x_{new}^T = [\Delta V_{PV}, \Delta i_{mp}, \Delta S_{C1}, \Delta I_{F1}, \Delta I_{ESS}, \Delta S_{C2}, \Delta I_{F2}, \Delta I_{EV}, \Delta V_{dc}, \Delta i_{Nd}, \Delta i_{Nq}, \Delta i_d, \Delta i_q, \Delta i_{Ld}, \Delta i_{Lq}, \Delta v_d, \Delta v_q, \Delta i_{dref}, \Delta U_d, \Delta i_{qref}, \Delta U_q, \Delta w_{PLL}, \Delta\theta_{PLL}, \Delta Q, \Delta V_{dc_s}]$ are states variable vector that represents the behavior of AC/DC hybrid microgrid-based EV charging infrastructure with a DSTATCOM controller. In this system, the DC microgrid states include ΔV_{PV} is the output voltage of the PV array; Δi_{mp} is the maximum output current of the PV array; ΔS_{C1}, ΔI_{F1} and ΔI_{ESS} are the state of charge (SOC), filtered current (low-frequency current dynamics), and current supplied to DC microgrid by ESS, respectively; ΔS_{C2}, ΔI_{F2}, and ΔI_{EV}, are the state of charge (SOC), filtered current (lowfrequency current dynamics), and current drawn for EV charging from DC microgrid, respectively and the DC bus voltage is denoted by ΔV_{dc}. For the AC grid states, Δi_{Nd} and Δi_{Nq} are d and q components of current supplied to the grid; Δi_d, and Δi_q represent the current supplied to both the AC grid and AC loads; Δi_{Ld}, and Δi_{Lq} are the current supplied to inductive AC load; Δv_d and Δv_q are the d and q components of AC bus voltage; and Δw_{PLL} and $\Delta \theta_{PLL}$ represent the frequency and phase angle deviations of the PLL, respectively; ΔQ is the reactive power at the AC terminal of the DC-AC converter and Δi_{dref}, ΔU_d, Δi_{qref} and ΔU_q are controller parameters of the DC-AC converter. The ΔV_{dc_s} denotes DC link voltage of DSTATCOM.

The control input vector $\Delta u^T = [\Delta d, \Delta d_{boost}, \Delta d_{buck}, \Delta V_{ESS}, \Delta V_{EV}, \Delta V_{DCref}, \Delta Q_{ref}, \Delta m., \ \Delta \delta]$ consists of various parameters that control different aspects of the DC microgrid-based EV charging infrastructure. These parameters include Δd the duty cycle of the PV array's boost converter; Δd_{boost} and Δd_{buck} are the duty cycles of the ESS converter and the EV's buck converter, respectively; ΔV_{ESS} and ΔV_{EV}, the voltage levels of the ESS and EV, respectively; ΔV_{DCref} is the reference value for the DC bus voltage; ΔQ_{ref} is the reference for reactive power at the AC side of the DC -AC converter; and Δm and $\Delta \delta$, the modulation index and phase angle control for the DSTATCOM. This control input vector enables precise regulation of the system's operation, ensuring efficient power flow and voltage stability within the microgrid.

The A matrix has the size of 25×25, while the B matrix has dimensions of 9×25, as detailed in the appendix. To represent the system in a homogeneous model for improved analysis of its dynamic performance, the state equation is written as

$$\Delta \dot{x}_{\text{new}} = A_H \Delta x_{\text{new}} \tag{8}$$

Where $A_H = (A_{new} - B_{\text{new}}\, k)$

In this context, the control input is defined as

$$u = -k x_{\text{new}}.$$

where the dimensions of u are 9×1 and k have dimensions of 9×25. To optimize system performance, particularly to reduce peak overshoot and settling time, a heuristic optimization approach (PSO) has been used to tune the control parameter of the state feedback control matrix k, improving the overall dynamic behaviour and stability of the system.

III. PARTICLE SWARM OPTIMIZATION

The Particle Swarm Optimization (PSO) algorithm, introduced by Kennedy and Eberhart in 1995 [22] [23], is a population-based optimization method inspired by natural swarm behaviour, like bird flocking and fish schooling. Known for its simplicity and fast convergence, the PSO uses a swarm of particles that explore the search space to find an optimal solution. Each particle maintains a position and velocity, tracking its personal best position (p_{best}) while the swarm monitors the best global position (g_{best}). Guided by these, particles iteratively update their positions and velocities to converge toward the optimal solution using the following equations

$$v_i^{t+1} = v_i^t + c_1 * r_1 \left(p_{\text{best}}^t - x_i^t\right) + c_2 * r_2 \left(g_{\text{best}}^t - x_i^t\right) \tag{9}$$

$$x_i^{t+1} = x_i^t + v_i^{t+1} \tag{10}$$

Here, v_i and x_i represent the velocity and position of the particle i, respectively; c_1 and c_2 are cognitive and social coefficients that determine the influence of the p_{best} and g_{best} on the particle's motion; and r_1 and r_2 are random values in the range [0, 1], introducing stochasticity into the search process. If a particle's current position provides a better value for the objective function $f(x_i)$ compared to its previous p_{best}, the p_{best} is updated accordingly.

$$f\left(x_i^t\right) < f\left(p_{\text{best}}\right) \tag{11}$$

$$p_{\text{best}} = x_i^t \tag{12}$$

In this paper, the ITAE (Integral of Time-weighted Absolute Error) performance criterion is adopted for controller parameter tuning. Compared with other error-based criteria such as ISE, IAE, and ITSE, ITAE offers distinct advantages: it not only minimizes the magnitude of error but also penalizes errors that persist for a longer duration by weighting them with time. This ensures improved transient response, reduced oscillations, and faster settling time, which are essential for stability in AC/DC hybrid microgrid and EV charging applications. In this work, the PSO algorithm [24] is applied to iteratively minimize the ITAE objective function, a performance metric specifically designed to reduce peak overshoot/undershoot and settling time of small-signal perturbations across all system states. The ITAE criterion is mathematically defined as:

$$F(e(t)) = ITAE = \int_0^\infty t|e(t)|dt \tag{13}$$

where $e(t)$ represents the error of small-signal perturbations in system states (Δx_{new}). Minimizing this objective ensures optimal tuning of the state feedback control matrix (k), enhancing system stability, dynamic performance, and damping of oscillations.

IV. KD CONTROL FOR PRECISE CONTROL OF AC/DC HYBRID MICROGRID

In dynamic systems, maintaining stable operation under varying operating conditions is often challenging when using conventional PI/PID controllers or fixed tuned parameters obtained from heuristic algorithms. To address this, a Knowledge Domain (KD) control framework is proposed — an adaptive and intelligent strategy that dynamically updates controller parameters in real time under changing operating scenarios [20], [25].

The core idea of KD control is to build a database of optimized controller parameters corresponding to different operating conditions. For each condition, controller parameters are pre-tuned and stored in the KD database. When the system encounters a new operating state, it rapidly maps the condition to the KD database, retrieves the relevant parameters, and applies them. This ensures precise, welldamped responses and enhanced stability without the need for continuous manual re-tuning.

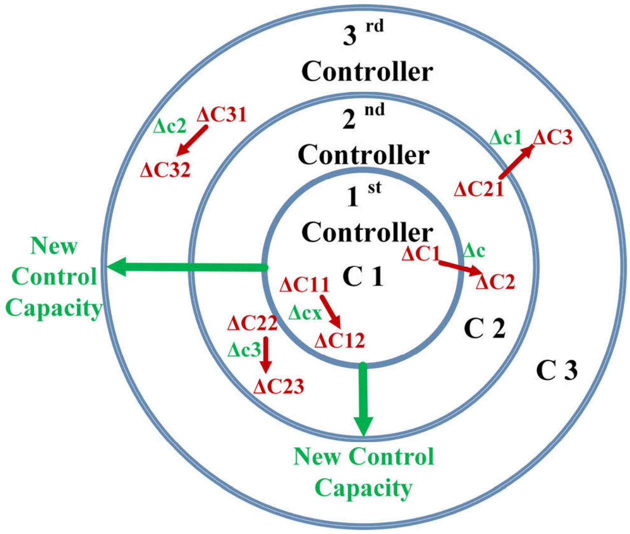

FIGURE 4. The knowledge domain control framework.

The KD control for various operating conditions, once converted into the designed controllers in terms of tuned parameters, becomes the specific controller structure for particular operating conditions. However, when other operating conditions are observed, the system again needs to be designed to provide a new dataset for new operating conditions as a new controller parameter. Therefore, changing system operating conditions and changing controller parameters can be built up with KD control. Now, the controller must work for a given set of operating conditions, with respect to the specific data domain in a KD framework shown in Fig. 4.

However, whenever there is change in operating conditions, the already tuned control parameter is available in KD database, so it will see the threshold of earlier operating conditions, and new operating conditions onset, and therefore it will shift to new operating conditions or new control architecture can be found by keeping the old parameters and assigning the new controller with new parameters, then this concept may be known as controller sharing or controller shifting.

Whenever new operating conditions are observed, respective operating conditions are mapped into the KD database, and accordingly, the data is retrieved, and the data is realized by the controller. Such controllers start working very precisely with a well-damped response. Therefore, such KD can be developed for various operating conditions with the controller flexibility. This controller's flexibility can be aided by the proposed KD control framework in terms of tuned controller parameters. Extension of the KD database for other changing dynamic conditions can also be realized on the same concept.

The KD control mitigates undesired performance of the controller by automatically updating the control parameters, quickly damping oscillations, and restoring stability. The KD control is realized using the PSO algorithm to generate and fine tuning of control parameters, particularly for the state feedback control matrix (k). The system incorporates a DSTATCOM to address dynamic oscillations initially. For example, during increased load demand on AC and DC buses, the DSTATCOM rapidly mitigates voltage and frequency fluctuations. In conjunction with the KD, the system then applies updated control parameters to further damp oscillations and improve stability.

The settings of the controllers are denoted as C1, C2, and C3, each corresponding to a specific control range. These settings can be extended to accommodate n controllers, enhancing system robustness. If a change in operating conditions (Δ L1) surpasses the capacity of the first controller (Δ C1), the second controller (Δ C2) provides supplementary control efforts, represented by $\Delta C2 \rightarrow \Delta C1 + \Delta$ c.

Fig. 4 illustrates the KD control framework, where concentric circles represent the control capacities of multiple controllers. The innermost circle denotes the capacity of the first controller (C1). If the operating parameters remain near the centre, the system retains sufficient control margin. However, as the parameters approach the circle's edge, the system becomes critical, requiring supplementary control efforts. When a perturbation exceeds the capacity of C1, additional controllers such as C2, C3 etc. activated, extending the control range and stabilizing the system. This hierarchical control strategy leverages the KD control to adapt control parameters dynamically, ensuring the stability of AC/DC hybrid microgrid and provide quality EV charging under dynamical varying operating conditions. By addressing both immediate oscillations and long-term stability needs, the KD concept facilitates efficient, reliable power delivery and continuous EV charging.

V. CONCEPT FOR DYNAMICAL CONTROLLER TUNING

The application of KD control requires dynamically updating controller parameters according to the system's current operating conditions. These parameters, stored in the KD database, enable precise state regulation and improved system stability. Fig. 5 illustrates the complete process, including KD database building, system pre-processing, and real-time application of KD control.

The KD control building block algorithm consists of three main stages:

1. Pre-Processing: The system checks whether the state deviations (Δx_{new}) are within predefined limits. If all deviations are within limits, no updates to the controller parameters are required.
2. KD Control Framework: When deviations exceed acceptable limits, the KD control framework retrieves the appropriate controller parameters from the KD

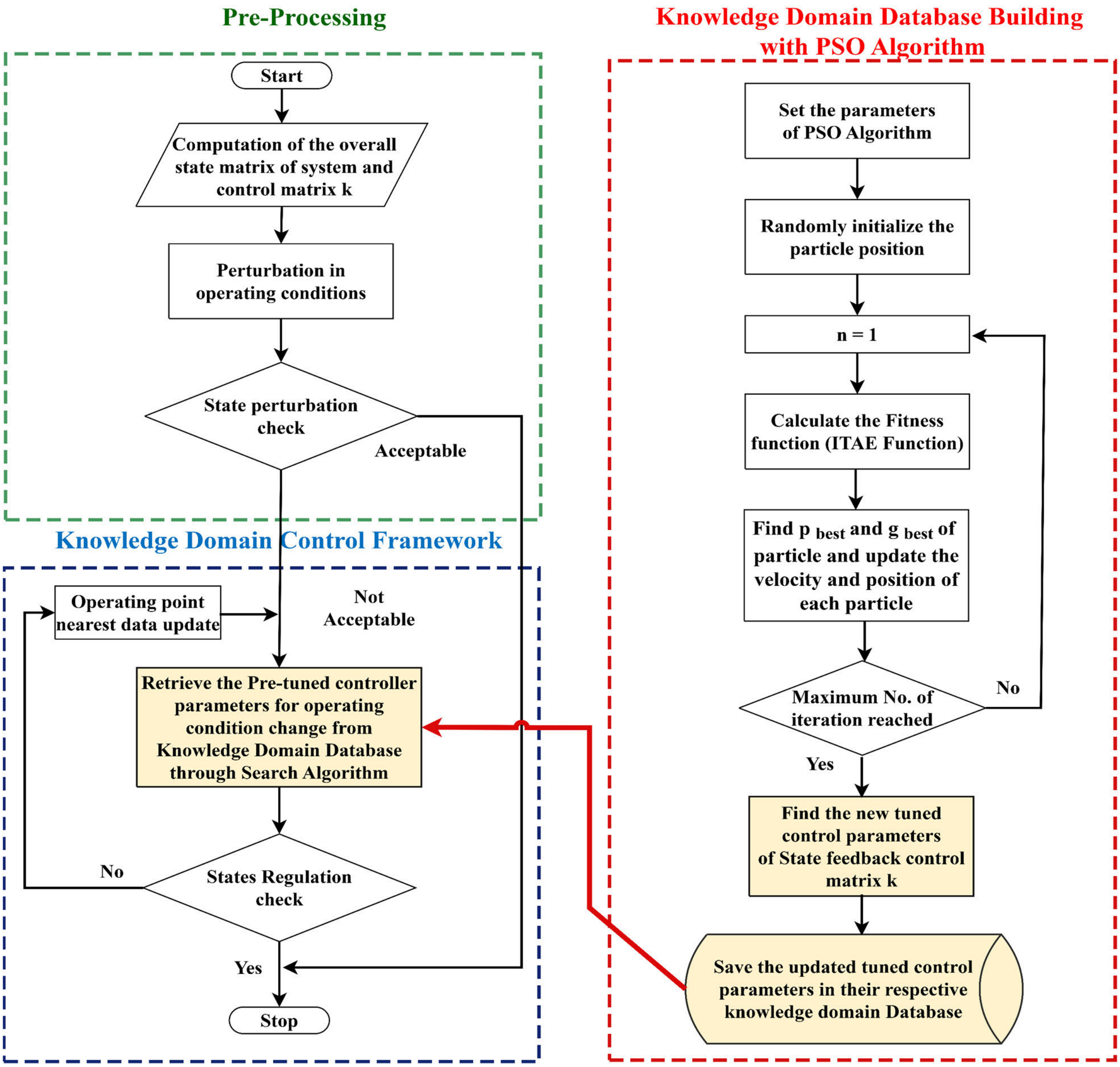

FIGURE 5. Knowledge domain control building block algorithm.

database based on current operating conditions. This update ensures proper state regulation, rapidly damps oscillations, and improves system stability.

3. KD Database Building: Using the PSO algorithm, a database of ready-to-use controller parameters is prepared offline for a wide range of operating conditions. The state feedback control matrix (k) is optimized offline using the ITAE criterion as the objective function to minimize state deviations. These optimized parameters are then stored in the KD database [20], [25].

During real-time operation, the system continuously monitors each state variable to ensure it remains within its predefined maximum and minimum thresholds. Ideally, small-signal perturbations (Δx_{new}) should converge to zero in the steady state. If any state exceeds its limits, controller switching is triggered. The KD framework searches the database for the most suitable controller parameters corresponding to current operating conditions. If exact parameters are unavailable, the framework uses nearby parameters, updates the controller structure, and verifies the state responses. This process is repeated iteratively until all states are within acceptable limits.

This dynamic mechanism allows the KD control to shift between controllers (e.g., C1 → C2) as illustrated in Fig. 4, extending the control range and ensuring system stability. The main limitation is that KD control is effective only as long as the system components and controllers can accommodate the required control range; beyond this range, hardware

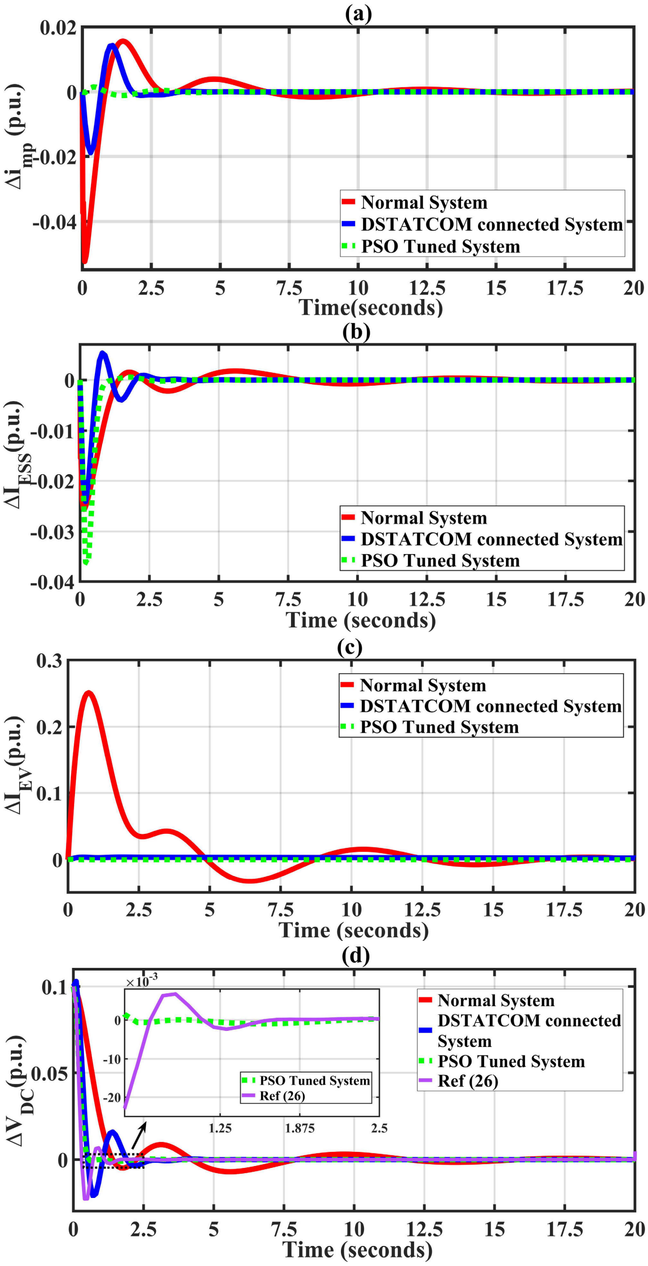

FIGURE 6. The response of DC side states without, with DSTATCOM, and PSO-tuned DSTATCOM integrated system under perturbed conditions (10% perturbation in DC bus voltage).

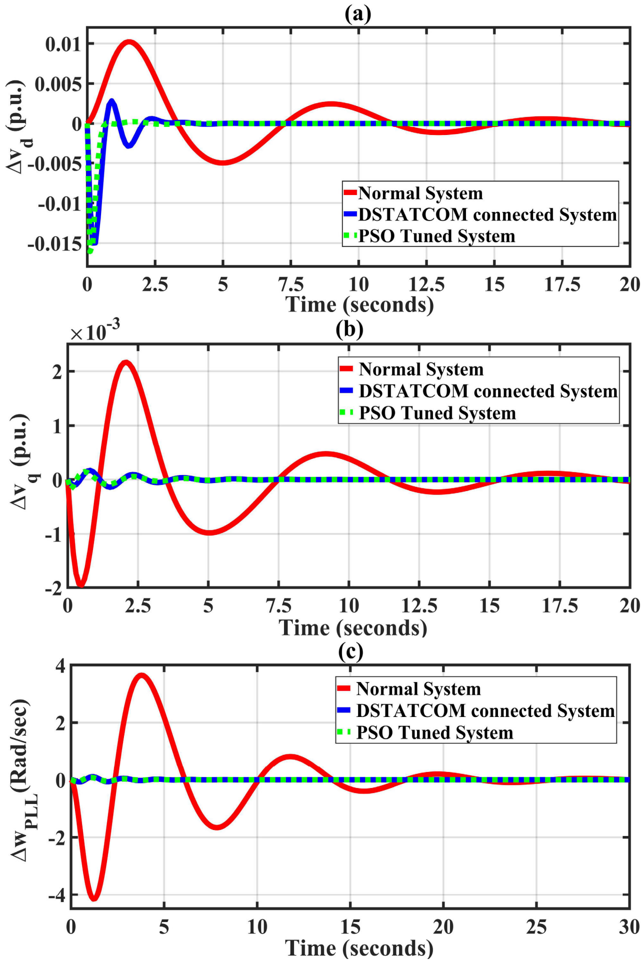

FIGURE 7. The response of the AC sides states without, with DSTATCOM, and PSO-tuned DSTATCOM under perturbed conditions (10% perturbation in DC bus voltage).

or device upgrades are necessary. By combining offline PSO-based optimization with real-time adaptive KD control, the framework achieves, efficient damping of oscillations, rapid stabilization during perturbation and consistent system performance providing quality EV charging under dynamically varying conditions.

VI. CASE STUDY AND RESULTS

The case study of the example system considered (Fig. 1) presents a DSTATCOM integrated AC/DC hybrid microgrid model for EV charging. The system has been represented in a state space framework. The overall system stability is evaluated using state perturbation analysis in terms of states regulation. Since the states collectively define the system's behavior, any perturbation in one state affects the others, making it essential to regulate all states simultaneously rather than individually. The system's resilience lies in its ability to restabilize the entire sub-system in response to dynamical changes, whether due to solar power deficits, surges in EV charging demand, ESS depletion, or AC grid disturbances.

The case study explores the system's performance under two categories: a) perturbed system condition and b) dynamic varying operating conditions. The results highlight the AC/DC hybrid microgrid's capability to maintain stability and ensure continuous EV charging.

A. PERTURBED SYSTEM CONDITION

To assess the effectiveness of DSTATCOM and PSO-tuned controller, the DC bus voltage is perturbed by 10%, which may occur due to fluctuations in EV charging load, variations in solar power or ESS power, or the AC grid's inability to maintain the DC bus voltage.

TABLE 1. Comparison of system states responses under 10 % DC bus voltage perturbation.

State	Normal System		DSTATCOM Connected System		PSO-tuned DSTATCOM-connected system	
	Overshoot / Undershoot (pu)	Settling time (s)	Overshoot / Undershoot (pu)	Settling time (s)	Overshoot / Undershoot (pu)	Settling time (s)
ΔV_{PV}	0.02	18	0.028	4.5	-0.002	4.5
Δi_{mp}	-0.052	15	-0.019	3.6	0.0015	3.6
ΔS_{C1}	1.8×10^{-6}	22	8.26×10^{-7}	4.5	1.4×10^{-6}	3.3
ΔI_{F1}	-0.023	19.3	-0.021	5	-0.033	3.6
ΔI_{ESS}	-0.025	16	-0.024	4.3	-0.036	1.4
ΔS_{C2}	4×10^{-4}	21	5.6×10^{-5}	0.7	1×10^{-7}	0.5
ΔI_{F2}	-0.25	20.4	4×10^{-3}	4.3	4×10^{-4}	0.4
ΔI_{EV}	0.25	17.6	9.7×10^{-5}	0.6	2×10^{-6}	0.2
ΔV_{dc}	**0.1**	**16**	**0.1**	**3**	**0.1**	**0.6**
Δi_{Nd}	-0.014	21.7	3.6×10^{-4}	11.6	-2.7×10^{-4}	9.2
Δi_{Nq}	-0.014	22	8.9×10^{-4}	11.7	-6.8×10^{-4}	9.3
Δi_d	-0.05	16.8	-0.077	4.3	-0.083	0.9
Δi_q	6×10^{-4}	20	-4.6×10^{-4}	5.4	-6.3×10^{-4}	3.2
Δi_{Ld}	4.5×10^{-3}	20.7	-6×10^{-4}	10.7	-5.2×10^{-4}	8.5
Δi_{Lq}	-0.019	22.3	0.031	5.1	0.034	3.4
Δv_d	0.01	19	-0.015	4.1	-0.016	0.7
Δv_q	2.1×10^{-3}	15.6	1×10^{-4}	5.7	1.6×10^{-4}	3.8
Δi_{dref}	-0.054	20	-0.067	5.1	-0.07	3.5
ΔU_d	-0.11	10.1	-0.05	4.4	0.037	2.9
Δi_{qref}	7.5×10^{-4}	21.6	4.5×10^{-4}	8.6	5.8×10^{-4}	6.3
ΔU_q	5.5×10^{-4}	18	2.8×10^{-4}	6.7	0.001	3.1
Δw_{PLL} (rad/sec)	-4.16	26	0.1	12.8	0.07	9.1
$\Delta \theta_{PLL}$ (rad/sec)	-5.66	28	-0.033	11.5	-0.028	9.3
ΔQ	9.5×10^{-4}	25	6×10^{-4}	6.6	5×10^{-4}	3.5
ΔV_{dc_S}	-	-	-0.22	5.5	-0.24	2.3

The results show how perturbations in the DC bus voltage state affect all other system states. These fluctuations cause significant oscillations in the system, which are subsequently damped out using DSTATCOM. It regulates the AC bus voltage by reactive power management.

This, in turn, stabilizes the AC bus voltage, as shown in Fig.7 (Δv_d and Δv_q states) which indirectly stabilizes the DC bus voltage through converter control and related states, so overall states are regulated, and system stability is improved.

The results indicate that perturbations in the DC bus voltage have a more pronounced impact on the DC microgrid states compared to the AC side states, as shown in Fig. 6. The implementation of the PSO tuned controller parameters significantly enhances system performance by rapidly damping oscillations, thereby reducing both settling time and peak overshoot/undershoot compared to other heuristic algorithms, such as the FA algorithm [26], due to faster convergence and a better balance between exploration and exploitation. The simulation results show that the settling time of the perturbed DC bus voltage state is reduced from 16 s (normal system response) to 3 s with the DSTATCOM integrated system response. It is further improved to 0.6 s with the PSO-optimized controller, whereas the FA-tuned controller achieves a settling time of 1.6 s, as illustrated in Fig. 6(d).

Table 1 presents a detailed comparison of system responses under the normal system, DSTATCOM-connected system, and the PSO-tuned DSTATCOM-connected system under 10% DC bus voltage perturbation. The table provides insights into each system state's dynamic behavior, illustrating how the DSTATCOM contributes to damping system oscillations and reducing settling time. Furthermore, the application of PSO-tuned controller parameters in the state-feedback control matrix (k) enhances these improvements, resulting in faster stabilization and better overall system performance.

B. DYNAMIC VARYING OPERATING CONDITIONS: CONTROL PARAMETER UPDATES USING THE KD CONTROL

The effectiveness and practicality of the proposed KD control framework is validated through real-time simulation using the OPAL-RT OP4512 simulator available in the Smart Grid Lab at IIT (BHU), Varanasi, as shown in Fig. 8. The experimental setup includes the OP4512 simulator (equipped with four Intel Xeon E3, 3.7 GHz cores), a host PC, and a LAN cable

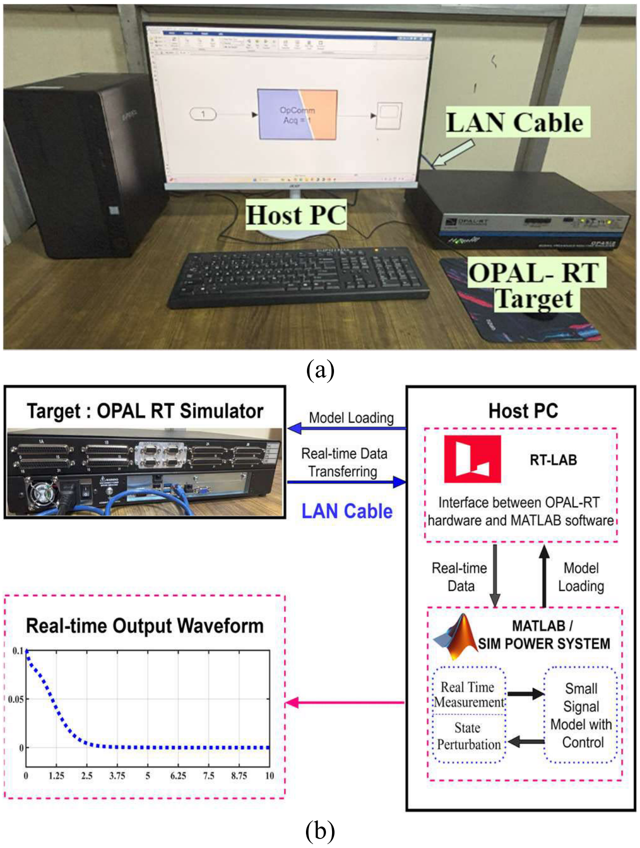

FIGURE 8. (a) Real-time experimental setup including the OPAL-RT target, the host PC, and a LAN cable for networking. (b) Real-time simulation process using OPAL-RT simulator.

for communication. The system operates on a Linux-based OS, with an Xilinx Kintex-7 410T FPGA handling the I/O operations. The RT-LAB software (v2024.3.0.21) provides the interface between MATLAB 2024.1 and the OPAL-RT platform, ensuring real-time execution of the SimPowerSystems model.

To implement the proposed KD control in real time, the MATLAB/SimPowerSystems model is loaded onto the OPAL-RT simulator via RT-LAB. During execution, realtime data is transmitted back to the MATLAB environment for monitoring and analysis. The SimPowerSystems model is structured into two subsystems: one dedicated to the main models for real-time simulation and the other for displays and variable parameters. After loading the model and receiving real-time data, waveforms are analysed within the SimPowerSystems environment to ensure accurate performance evaluation.

The case studies are divided into two parts: DC bus voltage perturbation and AC bus voltage perturbation. It is assumed that, before t = 0 s, the system experiences a 10% DC bus perturbation in both cases. To further illustrate the proposed KD control framework, an additional 10% DC bus perturbation is applied at t = 0 s for DC bus perturbation analysis. Similarly,

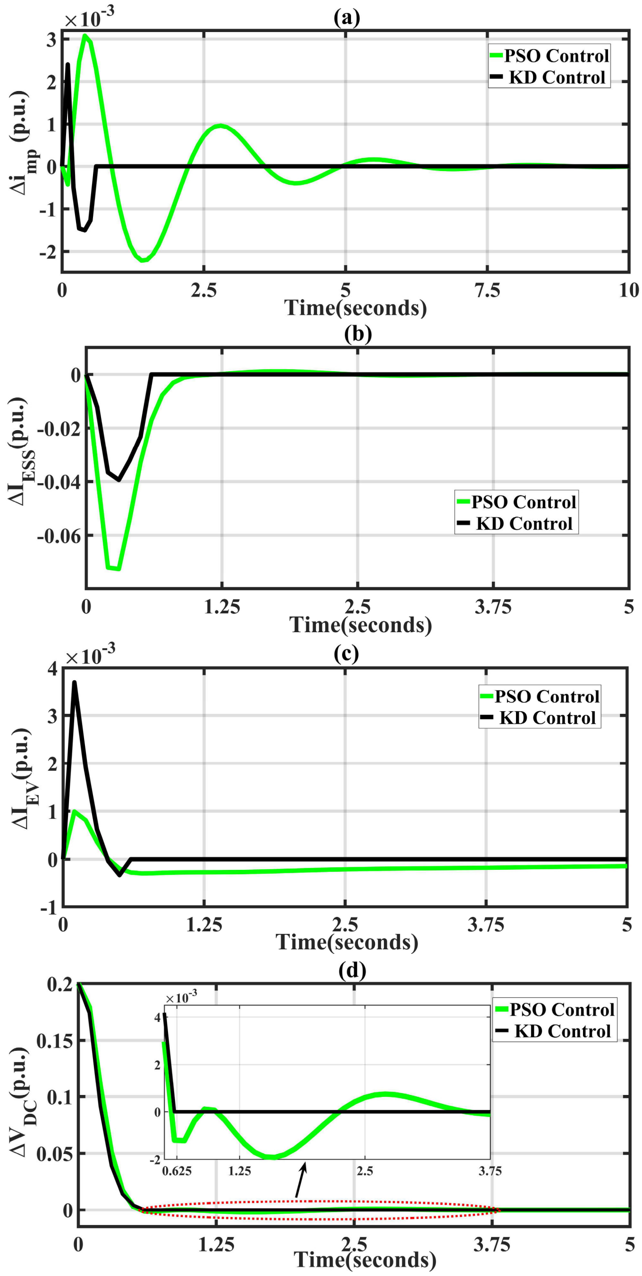

FIGURE 9. The response of the AC side states of the DSTATCOM integrated system under KD control, PSO-based control (without KD) for an additional 10% DC bus voltage perturbation over the existing operating condition.

for the AC bus perturbation analysis, a 10% perturbation is introduced in the Δvd states.

1) DC BUS VOLTAGE PERTURBATION

To evaluate the real-time practicality of the proposed KD control over the conventional heuristic algorithm (PSO control), a 10% DC bus voltage perturbation is introduced on top of the existing 10% perturbation in the system.

The DC bus voltage is considered because its variability can arise from solar power fluctuations, ESS power

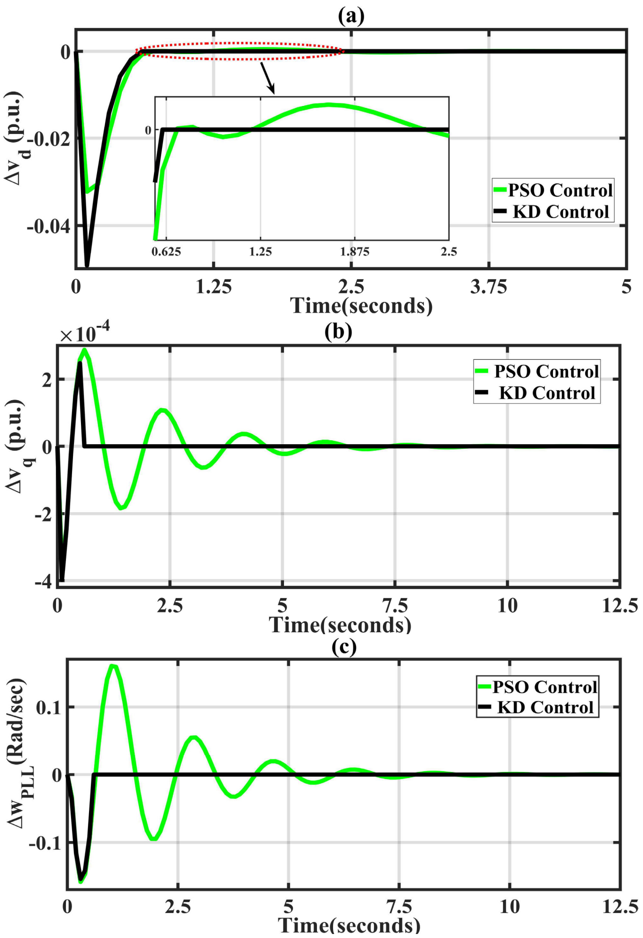

FIGURE 10. **The response of the AC side states of the DSTATCOM integrated system under KD control, PSO-based control (without KD) for an additional 10% DC bus voltage perturbation over the existing operating condition.**

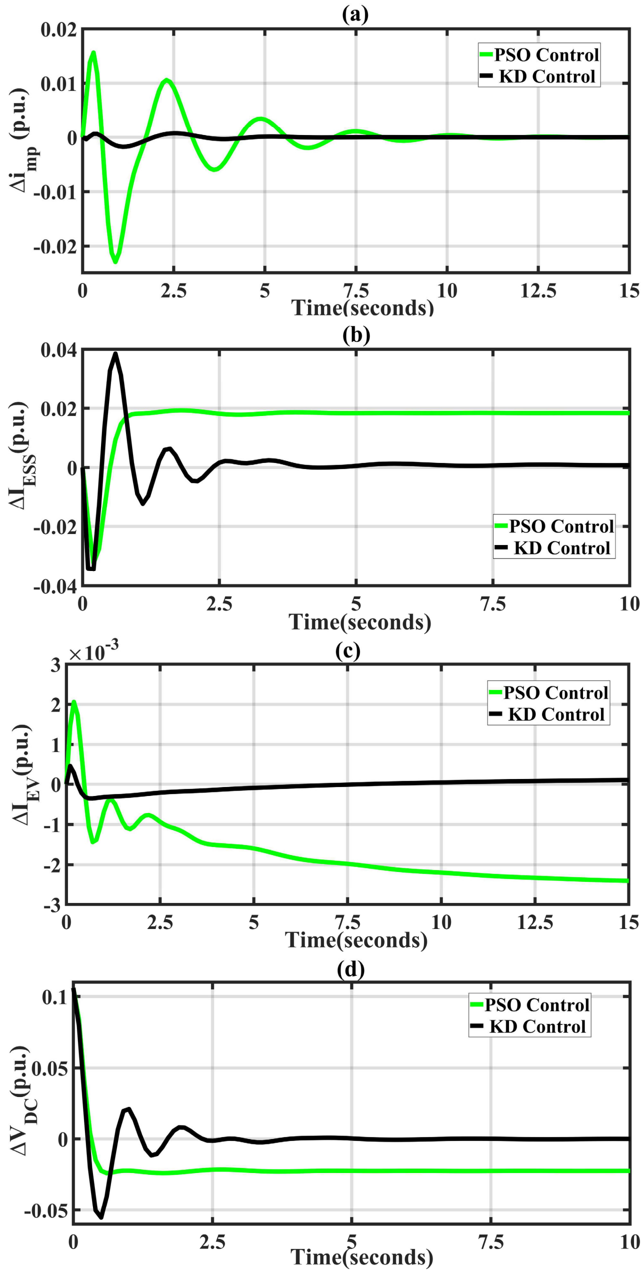

FIGURE 11. **The response of DC side states of the DSTATCOM integrated system under KD control, PSO-based control (without KD) for an additional 10% AC bus voltage perturbation over the existing operating condition.**

variability, changes in EV charging demand, and the limited capacity of the AC grid to handle these variations. Introducing this additional perturbation makes the case study closely representative of real-world operating conditions.

In this case, the DC bus voltage initially experiences a 10% perturbation before t = 0 s. At t = 0 s, an additional 10% perturbation is applied, resulting in amplified oscillations and increased settling time. Since the perturbation directly impacts the DC bus, the DC-side states exhibit more pronounced oscillations than the AC side, as shown in Fig. 9. Initially, the DSTATCOM mitigates some of these oscillations by regulating the AC bus voltage. However, due to its limited control capability, certain oscillations persist. In such cases, the KD control framework evaluates the parameter control range. If oscillations persist, the proposed KD control swiftly updates the controller parameters in real time by retrieving the appropriate values from the KD database based on current system operating conditions. This instantaneous adaptation distinguishes KD control from conventional heuristic algorithms (PSO control, etc.), which require additional time for re-optimization before applying new parameters. Such delays often risk exacerbating oscillations and can even lead to performance degradation or system collapse.

The simulation results validate the superiority of the KD control approach over PSO control. By employing KD-based parameter adaptation, system oscillations are rapidly suppressed, settling time is reduced, and AC/DC bus voltages are effectively regulated, thereby significantly enhancing overall system stability. Specifically, the settling time of the perturbed DC bus voltage decreases from 4 s with PSO control to

TABLE 2. Comparison of system states responses.

States	10 % Additional DC Bus Voltage Perturbation				10 % Additional AC Bus Voltage Perturbation			
	PSO Control		KD Control		PSO Control		KD Control	
	Overshoot / Undershoot (pu)	Settling time (s)	Overshoot / Undershoot (pu)	Settling time (s)	Overshoot / Undershoot (pu)	Settling time (s)	Overshoot / Undershoot (pu)	Settling time (s)
ΔV_{PV}	-4.6×10^{-3}	9.8	12×10^{-4}	0.6	4.8×10^{-3}	11	3.2×10^{-3}	9
Δi_{mp}	3×10^{-3}	9.4	2×10^{-3}	0.6	-23×10^{-3}	10.5	-1.7×10^{-3}	3.5
ΔS_{C1}	2.8×10^{-6}	4.2	1.27×10^{-6}	0.6	-7.8×10^{-5}	6.2	-0.8×10^{-5}	4
ΔI_{F1}	-0.066	4.5	-0.035	0.6	-0.028	6.2	0.038	4.2
ΔI_{ESS}	-0.072	2.4	-0.039	0.6	-0.032	5	0.038	6.2
ΔS_{C2}	2×10^{-7}	4.2	5.6×10^{-6}	0.6	9.8×10^{-7}	12.5	-9.2×10^{-5}	5.9
ΔI_{F2}	-0.0008	4.2	-0.002	0.6	3.2×10^{-4}	12.5	2.5×10^{-3}	5.9
ΔI_{EV}	1×10^{-3}	3.8	3.7×10^{-3}	0.6	2×10^{-3}	11.5	0.4×10^{-3}	5.6
ΔV_{dc}	**0.2**	**4**	**0.2**	**0.6**	**0.1**	**5**	**0.1**	**2.5**
Δi_{Nd}	-5.4×10^{-4}	10.7	-5×10^{-4}	0.7	-1.2×10^{-3}	10.8	-1.2×10^{-3}	9.1
Δi_{Nq}	1.2×10^{-3}	9.9	2×10^{-3}	0.6	-5×10^{-3}	11.2	-5×10^{-3}	9.3
Δi_{d}	-0.167	3.4	-0.25	0.6	-0.1	8.2	-0.078	5
Δi_{q}	-12.6×10^{-4}	6	-1.1×10^{-3}	0.6	-4×10^{-3}	8.2	-3.4×10^{-3}	6.9
Δi_{Ld}	-10.5×10^{-4}	9.9	-6.5×10^{-4}	0.7	-1.8×10^{-3}	10.6	-2×10^{-3}	8.4
Δi_{Lq}	0.068	3.4	0.104	0.6	0.04	6.9	0.032	5.9
Δv_{d}	-0.032	2.4	-0.049	0.6	0.1	6.8	0.1	0.7
Δv_{q}	-3.5×10^{-4}	8.3	-4×10^{-4}	0.6	-7.5×10^{-4}	7.8	-5.7×10^{-4}	6.5
Δi_{dref}	-0.14	3.6	-0.165	0.6	-0.08	7.6	-0.06	5.3
ΔU_{d}	0.075	3.7	0.08	0.6	0.047	5.5	0.076	5.2
Δi_{qref}	-1.2×10^{-3}	7.1	-1.1×10^{-3}	0.6	-3×10^{-3}	5.8	-2.8×10^{-3}	5.4
ΔU_{q}	-2.4×10^{-3}	4	-1.5×10^{-3}	0.6	5.3×10^{-3}	4.7	5×10^{-4}	3.3
Δw_{PLL} (rad/sec)	0.154	8.8	-0.16	0.6	-0.38	10.2	-0.38	9.1
$\Delta\theta_{PLL}$ (rad/sec)	-0.056	10.1	-0.05	0.6	-0.187	9.1	-0.18	8.5
ΔQ	0.0011	6.4	0.002	0.7	3×10^{-3}	6.2	3.5×10^{-3}	5.6
ΔV_{dc_S}	-0.492	4.6	-0.723	0.6	-0.24	7.1	-0.2	5.5

0.6 s with KD control, ensuring improved voltage regulation and enabling high-quality EV charging.

2) AC BUS VOLTAGE PERTURBATION

Similar to the DC bus voltage perturbation analysis, a 10% AC bus voltage perturbation is introduced in Avd state at t = 0 s, in addition to the existing 10% perturbation in DC bus voltage state present before t = 0 s. This scenario is considered because AC bus voltage fluctuations often arise due to high load demand at both AC and DC buses or the inability of the AC grid to supply sufficient power. Introducing this additional AC perturbation makes the case study closely representative of real-world operating conditions where both demand and generation vary dynamically.

The combined AC and DC bus voltage perturbations affect both AC and DC side states, producing pronounced oscillations due to supply-demand mismatches, as illustrated in Fig. 11 and Fig.12. DSTATCOM initially compensates part of these oscillations by regulating the AC bus voltage; however, its limited control capability allows significant oscillations to persist.

At this stage, the proposed KD control plays a critical role by dynamically updating the controller parameters of the state feedback matrix (K) from the KD database according to the system's current operating conditions. Under such conditions, the superiority of KD control over PSO-based control becomes evident, as illustrated in Fig. 11(b), 11(c), 11(d), and Fig. 12(a). The results show that when the operating condition changes, PSO control fails to provide precise state regulation and exhibits steady-state error. Specifically, with PSO, the perturbed DC bus voltage state experiences a steady-state error of approximately 3% with a settling time of 5 s, and under larger perturbations, it may even become unstable or fail altogether due to delays in reoptimization. In contrast, the proposed KD control completely eliminates the steady-state error and reduces the settling time to 2.5 s. This significant improvement is achieved through immediate parameter updates retrieved from the KD database, enabling rapid damping and precise regulation of both AC and DC bus voltages.

Table 2 presents a detailed comparison of system responses under KD control versus PSO control, highlighting each state's dynamic behaviour with respect to settling time, overshoot/ undershoot. The results demonstrate the superior effectiveness of KD control in enhancing system stability under dynamically varying operating conditions. For larger

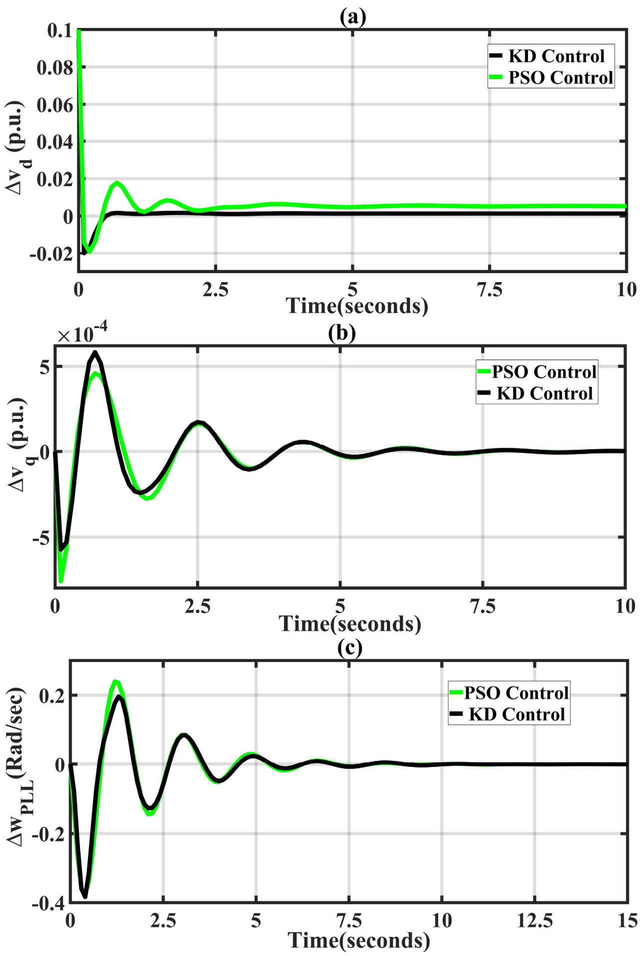

FIGURE 12. The response of AC side states of the DSTATCOM integrated system under KD control, PSO-based control (without KD) for an additional 10% AC bus voltage perturbation over the existing operating condition.

perturbations, PSO control may fail because it provides offline-tuned controller parameters only once. Under changing operating conditions, PSO requires additional time to re-optimize the parameters, making it unsuitable for highly variable scenarios. Similarly, conventional PI and PID controllers are inadequate for dynamically tuning controller parameters in system.

In contrast, the proposed KD control intelligently adapts to varying conditions, providing faster settling, reduced oscillations, and improved stability for both subsystems and the overall system. Built upon a robust state-space model, the framework seamlessly integrates new subsystem data, whether in system matrices, control matrices, or sub-state matrices, allowing the model to expand without compromising stability. As the system grows in size and complexity, KD control recalibrates parameters with precision, ensuring optimal performance. This innovative approach guarantees that even larger and more intricate systems maintain flexible, efficient, and future-ready control, while achieving unified stability across all subsystems.

TABLE 3. System parameters.

Parameters	Value
PV Output power	293 kW
Energy Storage (ES) and EV's battery voltage	500 V
Rated Capacity of ESS	2 kAh
Rated Capacity of EV	0.2 kAh
AC Grid Capacity	1 MW and 0.1 MVAR
AC load	1.9 MW and 0.14 MVAR
AC Bus Voltage	600 V
DC Bus Voltage	1000 V
Number of particles and iterations in the PSO algorithm, respectively	100,60

VII. CONCLUSION

This paper proposes a KD-based control for a DSTATCOM-integrated AC/DC hybrid microgrid designed for electric vehicle (EV) charging applications. The proposed control effectively addresses challenges arising from dynamic load variations, solar intermittency, and grid disturbances by combining offline controller parameter optimization using PSO with instantaneously controller parameter updates based on current operating conditions. The DSTATCOM plays a crucial role in regulating the AC bus voltage and indirectly stabilizing the DC bus voltage, ensuring uninterrupted and high-quality EV charging.

A detailed small-signal model has been developed to analyse interactions among all system components, including the PV array, ESS, EV loads, and DSTATCOM with associated converters. The stability analysis was conducted using state perturbation studies, confirming system stability in terms of precise state regulation. A 10% DC bus voltage state perturbation demonstrates how the DSTATCOM and PSO-optimized controller gains reduce oscillations and settling time. For instance, the settling time of a perturbed DC bus voltage decreased from 16 s to 3 s with DSTATCOM integration and further to 0.9 s with PSO-tuned controller parameters under a 10% DC bus voltage perturbation.

Experimental validation of the KD control versus PSO control was performed under 10% AC and DC bus voltage perturbations, on top of existing 10% DC bus voltage perturbations, to emulate dynamic variations. Simulation results confirm the KD control's effectiveness in rapidly stabilizing system dynamics, achieving a 78% reduction in settling time, from 4 s to 0.6 s under 20% DC bus perturbation, and from 5 s to 2.5 s under combined 10% Vdc and 10% Vac perturbation.

The proposed control ensures safe converter operation, consistent voltage regulation across AC and DC buses, and high-quality EV charging under adverse conditions. Integrating KD-based control with offline PSO optimization provides a robust, scalable, and intelligent solution for future EV-integrated smart microgrids, enhancing reliability, resiliency, and energy sustainability.

$$A_{11}=\begin{bmatrix} a_{S11} & a_{S12} & 0 & 0 & 0 & 0 & 0 & 0 & 0 & 0 & 0 & \\ a_{S21} & 0 & 0 & 0 & 0 & 0 & 0 & 0 & a_{S22} & 0 & 0 & \\ 0 & 0 & a_{ES11} & 0 & a_{ES12} & 0 & 0 & 0 & 0 & 0 & 0 & \\ 0 & 0 & 0 & a_{ES21} & a_{ES22} & 0 & 0 & 0 & 0 & 0 & 0 & \\ 0 & 0 & 0 & 0 & a_{ES31} & 0 & 0 & 0 & a_{ES32} & 0 & 0 & 0(8*14) \\ 0 & 0 & 0 & 0 & 0 & a_{EV11} & 0 & a_{EV12} & 0 & 0 & 0 & \\ 0 & 0 & 0 & 0 & 0 & 0 & a_{EV21} & a_{EV22} & 0 & 0 & 0 & \\ 0 & 0 & 0 & 0 & 0 & 0 & 0 & a_{EV31} & a_{EV32} & 0 & 0 & \end{bmatrix}_{8\times 25}$$

$$A_{21}=\begin{bmatrix} 0 & a_{21} & 0 & 0 & a_{22} & 0 & 0 & a_{23} & a_{24} & 0 & 0 & a_{25} & a_{26} & 0 & 0 & a_{27} & a_{28} & 0 & a_{29} & 0 & a_{210} & a_{211} & 0 & 0 & 0 \\ 0 & 0 & 0 & 0 & 0 & 0 & 0 & 0 & 0 & a_{31} & a_{32} & 0 & 0 & 0 & 0 & a_{33} & 0 & 0 & 0 & 0 & 0 & a_{34} & a_{35} & 0 & 0 \\ 0 & 0 & 0 & 0 & 0 & 0 & 0 & 0 & 0 & a_{41} & a_{42} & 0 & 0 & 0 & 0 & 0 & a_{43} & 0 & 0 & 0 & 0 & a_{44} & a_{45} & 0 & 0 \\ & & & & & & & & & & & 0 & 0 & 0 & 0 & 0 & 0 & 0 & a_{51} & 0 & 0 & 0 & 0 & 0 & 0 \\ & & & & & 0 & & & & & 0 & 0 & 0 & 0 & 0 & 0 & 0 & 0 & 0 & a_{61} & 0 & 0 & 0 & 0 & \\ & & & & & & & & & & 0 & 0 & a_{71} & 0 & a_{72} & 0 & 0 & 0 & 0 & 0 & a_{73} & 0 & 0 & 0 & \\ & & & & & & & & & & & 0 & 0 & 0 & a_{81} & 0 & a_{82} & 0 & 0 & 0 & 0 & a_{83} & 0 & 0 & 0 \end{bmatrix}_{7\times 25}$$

$$A_{31}=\begin{bmatrix} 0 & 0 & 0 & 0 & 0 & 0 & 0 & 0 & 0 & a_{91} & 0 & a_{92} & 0 & a_{93} & 0 & a_{94} & a_{95} & 0 & 0 & 0 & 0 & a_{96} & 0 & 0 \\ 0 & 0 & 0 & 0 & 0 & 0 & 0 & 0 & 0 & 0 & a_{101} & 0 & a_{102} & 0 & a_{103} & a_{104} & a_{105} & 0 & 0 & 0 & 0 & a_{106} & 0 & 0 \\ 0 & a_{111} & 0 & 0 & a_{112} & 0 & 0 & a_{113} & a_{114} & 0 & 0 & a_{115} & a_{116} & 0 & 0 & a_{117} & a_{118} & 0 & a_{119} & 0 & a_{1110} & 0 & 0 & 0 \\ 0 & a_{121} & 0 & 0 & a_{122} & 0 & 0 & a_{123} & a_{124} & 0 & 0 & a_{125} & a_{126} & 0 & 0 & a_{127} & a_{128} & a_{129} & a_{1210} & 0 & a_{1211} & 0 & 0 & 0 \\ 0 & 0 & 0 & 0 & 0 & 0 & 0 & 0 & 0 & a_{131} & a_{132} & a_{133} & a_{134} & a_{135} & a_{136} & a_{137} & a_{138} & 0 & a_{139} & 0 & a_{1310} & a_{1311} & 0 & a_{1312} \\ 0 & 0 & 0 & 0 & 0 & 0 & 0 & 0 & 0 & a_{141} & a_{142} & a_{143} & a_{144} & a_{145} & a_{146} & a_{147} & a_{148} & 0 & a_{149} & a_{1410} & a_{1411} & a_{1412} & 0 & a_{1413} \\ 0 & 0 & 0 & 0 & 0 & 0 & 0 & 0 & 0 & 0 & a_{151} & 0 & a_{152} & 0 & a_{153} & a_{154} & a_{155} & 0 & 0 & 0 & 0 & a_{156} & 0 & 0 \\ 0 & 0 & 0 & 0 & 0 & 0 & 0 & 0 & 0 & 0 & 0 & 0 & 0 & 0 & 0 & 0 & 0 & 0 & 0 & 0 & 0 & a_{161} & 0 & 0 \\ 0 & 0 & 0 & 0 & 0 & 0 & 0 & 0 & 0 & a_{171} & a_{172} & a_{173} & a_{174} & a_{175} & a_{176} & a_{177} & a_{178} & 0 & a_{179} & 0 & a_{1710} & a_{1711} & 0 & 0 \\ 0 & 0 & 0 & 0 & 0 & 0 & 0 & 0 & 0 & 0 & 0 & a_{181} & a_{182} & 0 & 0 & 0 & 0 & 0 & 0 & 0 & 0 & 0 & 0 & 0 \end{bmatrix}_{10*25}$$

The B matrix is

$$B=\begin{bmatrix} 0 & b_{s21} & 0 & 0 & 0 & 0 & 0 & 0 & b_{21} & & b_{11,1} & b_{12,1} & 0 & 0 & 0 & 0 & 0 & 0 \\ 0 & 0 & 0 & 0 & b_{es31} & 0 & 0 & 0 & b_{22} & & b_{11,2} & b_{12,2} & 0 & 0 & 0 & 0 & 0 & 0 \\ 0 & 0 & 0 & 0 & 0 & 0 & 0 & b_{ev31} & b_{23} & & b_{11,3} & b_{12,3} & 0 & 0 & 0 & 0 & 0 & 0 \\ 0 & 0 & 0 & 0 & b_{es32} & 0 & 0 & 0 & 0 & & 0 & 0 & 0 & 0 & 0 & 0 & 0 & 0 \\ 0 & 0 & 0 & 0 & 0 & 0 & 0 & b_{ev32} & 0 & 0_{(9\times 8)} & 0 & 0 & 0 & 0 & 0 & 0 & 0 & 0 \\ 0 & 0 & 0 & 0 & 0 & 0 & 0 & 0 & 0 & & b_{11,4} & b_{12,4} & 0 & 0 & 0 & 0 & 0 & 0 \\ 0 & 0 & 0 & 0 & 0 & 0 & 0 & 0 & 0 & & 0 & 0 & b_{13,1} & b_{14,1} & 0 & 0 & 0 & 0 \\ 0 & 0 & 0 & 0 & 0 & 0 & 0 & 0 & 0 & & 0 & 0 & 0 & 0 & 0 & 0 & 0 & 0 \\ 0 & 0 & 0 & 0 & 0 & 0 & 0 & 0 & 0 & & 0 & 0 & 0 & 0 & 0 & 0 & 0 & 0 \\ & & & & & & & & & & b_{18,1} & & & & & & & \end{bmatrix}^{T}_{9\times 25}$$

APPENDIX

The A matrix is defined as $A=\begin{bmatrix}[A_{11}]_{8\times 25}\\ [A_{21}]_{7\times 25}\\ [A_{31}]_{10\times 25}\end{bmatrix}_{25*25}$, where as shown in the equations at the top of the page.

REFERENCES

[1] G. Rajendran, C. A. Vaithilingam, N. Misron, K. Naidu, and M. R. Ahmed, "A comprehensive review on system architecture and international standards for electric vehicle charging stations," *J. Energy Storage*, vol. 42, Oct. 2021, Art. no. 103099.

[2] B. Faujdar and R. K. Pandey, "PV—Energy storage based EV charging infrastructure: Performance analysis," in *Proc. 23rd Nat. Power Syst. Conf.*, India, Dec. 2024, pp. 1–6.

[3] Faujdar, Babita, and R. K. Pandey, "DC microgrid based EV charging infrastructure-PSO controller tuning for optimal response," Presented at the IEEE PES General Meeting, Austin, TX, USA, 2025.

[4] M. Sithambaram, P. Rajesh, F. H. Shajin, and I. Raja Rajeswari, "Grid connected photovoltaic system powered electric vehicle charging station for energy management using hybrid method," *J. Energy Storage*, vol. 108, Feb. 2025, Art. no. 114828.

[5] M. M. Mahfouz and M. R. Iravani, "Grid-integration of battery-enabled DC fast charging station for electric vehicles," *IEEE Trans. Energy Convers.*, vol. 35, no. 1, pp. 375–385, Mar. 2020.

[6] A. Elsanabary, K. Khairullah, N. F. A. Aziz, and S. Mekhilef, "Power management and optimized control of hybrid PV-BESS-grid integrated fast EV charging stations," *J. Energy Storage*, vol. 90, Jun. 2024, Art. no. 111802.

[7] H. Yuan, H. Xin, D. Wu, W. Wang, and Y. Zhou, "Small-signal stability assessment of multi- converter-based-renewable systems with STATCOMs based on generalized short-circuit ratio," *IEEE Trans. Energy Convers.*, vol. 37, no. 4, pp. 2889–2902, Dec. 2022.

[8] H. Bakir and A. A. Kulaksiz, "Modelling and voltage control of the solar-wind hybrid micro-grid with optimized STATCOM using GA and BFA," *Eng. Sci. Technol., Int. J.*, vol. 23, no. 3, pp. 576–584, Jun. 2020.

[9] N. K. Saxena, W. D. Gao, A. Kumar, S. Mekhilef, and V. Gupta, "Frequency regulation for microgrid using genetic algorithm and particle swarm optimization tuned STATCOM," *Int. J. Circuit Theory Appl.*, vol. 50, no. 9, pp. 3231–3250, Sep. 2022.

[10] S. Chakraborty, S. Mukhopadhyay, and S. K. Biswas, "Optimal placement of PV-DSTATCOM based EV charging stations with dynamic pricing," *IEEE Trans. Ind. Appl.*, vol. 59, no. 6, pp. 7092–7102, Nov. 2023.

[11] V. Vutla and V. Chintham, "Multi-objective optimal planning of rapid charging stations, distributed generators, and D-STATCOM in coupled networks considering waiting time," *Energy Sour., A, Recovery, Utilization, Environ. Effects*, vol. 47, no. 1, pp. 526–546, Jun. 2025.

[12] K. K. Nandini and N. S. Jayalakshmi, "A combined approach to evaluate power quality and grid dependency by solar photovoltaic based electric vehicle charging station using hybrid optimization," *J. Energy Storage*, vol. 84, Apr. 2024, Art. no. 110967.

[13] N. Ghasemi, M. Ghanbari, and R. Ebrahimi, "Intelligent and optimal energy management strategy to control the micro-grid voltage and frequency by considering the load dynamics and transient stability," *Int. J. Electr. Power Energy Syst.*, vol. 145, Feb. 2023, Art. no. 108618.

[14] P. He, Q. Fang, H. Jin, Y. Ji, Z. Gong, and J. Dong, "Coordinated design of PSS and STATCOM-POD based on the GA-PSO algorithm to improve the stability of wind-PV-thermal-bundled power system," *Int. J. Electr. Power Energy Syst.*, vol. 141, Oct. 2022, Art. no. 108208.

[15] H. Yuan, L. Huang, H. Gao, D. Zheng, D. Wu, J. Xing, R. Diao, and H. Xin, "Robust adaptive control of STATCOMs to mitigate inverter-based-resource (IBR)-induced oscillations," *IEEE Trans. Sustain. Energy*, vol. 16, no. 1, pp. 3–16, Jan. 2025.

[16] M. K. Senapati, C. Pradhan, S. R. Samantaray, and P. K. Nayak, "Improved power management control strategy for renewable energy-based DC micro-grid with energy storage integration," *IET Gener., Transmiss. Distribution*, vol. 13, no. 6, pp. 838–849, Mar. 2019.

[17] M. K. Senapati, O. Al Zaabi, K. Al Hosani, K. Al Jaafari, C. Pradhan, and U. Ranjan Muduli, "Advancing electric vehicle charging ecosystems with intelligent control of DC microgrid stability," *IEEE Trans. Ind. Appl.*, vol. 60, no. 5, pp. 7264–7278, Sep. 2024.

[18] M. K. Senapati, C. Pradhan, S. Padmanaban, and O. A. Zaabi, "Photovoltaic MPPT performance adaptability to partial shading resilience and load variations with modified adaptive Jaya optimization," *IEEE Trans. Consum. Electron.*, vol. 71, no. 1, pp. 734–747, Feb. 2025.

[19] U. Hussan, A. Waheed, H. Bilal, H. Wang, M. Hassan, I. Ullah, J. Peng, and M. Hosseinzadeh, "Robust maximum power point tracking in PV generation system: A hybrid ANN-backstepping approach with PSO-GA optimization," *IEEE Trans. Consum. Electron.*, vol. 71, no. 2, pp. 6016–6026, May 2025.

[20] R. K. Pandey and D. K. Gupta, "Knowledge domain states mapping concept for controller tuning in an interconnected power network," *Int. J. Electr. Power Energy Syst.*, vol. 80, pp. 160–170, Sep. 2016.

[21] N. G. Hingorani and L. Gyugyi, *Understanding FACTS: Concepts and Technology of Flexible AC Transmission Systems*. Piscataway, NJ, USA: IEEE Press, 1999.

[22] R. Eberhart and J. Kennedy, "A new optimizer using particle swarm theory," in *Proc. 6th Int. Symp. Micro Mach. Human Sci.*, Jun. 1995, pp. 39–43.

[23] F. Marini and B. Walczak, "Particle swarm optimization (PSO). A tutorial," *Chemometric Intell. Lab. Syst.*, vol. 149, pp. 153–165, Dec. 2015.

[24] A. R. Jordehi, "Particle swarm optimisation (PSO) for allocation of FACTS devices in electric transmission systems: A review," *Renew. Sustain. Energy Rev.*, vol. 52, pp. 1260–1267, Dec. 2015.

[25] R. K. Pandey and D. K. Gupta, "Intelligent multi-area power control: Dynamic knowledge domain inference concept," *IEEE Trans. Power Syst.*, vol. 32, no. 6, pp. 4310–4318, Nov. 2017.

[26] Faujdar, Babita, and R. K. Pandey, "STATCOM integrated DC microgrid-based EV charging infrastructure–FA controller tuning for optimal response," Presented at the IEEE 5th Int. Conf. Sustain. Energy Future Electr. Transp., 2025.

BABITA FAUJDAR (Graduate Student Member, IEEE) received the master's degree in electrical engineering from Punjab Engineering College, Chandigarh, India, in 2021. She is currently pursuing the Ph.D. degree in electrical engineering with the Department of Electrical Engineering, Indian Institute of Technology (BHU), Varanasi, India. Her primary research interests include control of power systems, FACTS devices, application of heuristic algorithms, and energy management.

RAJENDRA KUMAR PANDEY (Senior Member, IEEE) received the Ph.D. degree in electrical engineering from Indian Institute of Technology, Kanpur, India, in 1992. He is currently a Professor of electrical engineering with IIT (BHU), Varanasi, India. His research interests include power oscillation damping, FACTS controller design, HVdc system studies, and smart energy grids.